www.czasopisma.pan.pl PAN POLSKA AKADEMIA NAUK www.journals.pan.pl

Arch. Metall. Mater. **65** (2020), 1, 185-192

DOI: 10.24425/amm.2019.131113

D. KAPINOS[1*], M. SZYMANEK[1], B. AUGUSTYN[1], S. BOCZKAL[1],
W. SZYMAŃSKI[1], T. TOKARSKI[2], J. LELITO[3]

THE EFFECT OF RARE EARTH ADDITION ON MICROSTRUCTURE AND MECHANICAL PROPERTIES OF THE RAPIDLY SOLIDIFIED Al-Si AND Al-Si-Ni ALLOYS

The article presents research aimed at determining the effect of adding rare earth elements to near-eutectic Al-Si and Al-Si-Ni alloys on the microstructure and mechanical properties of the obtained products. Material for the research was prepared using a melt spinner – a device used for rapid crystallization, casting thin ribbons, which were then subjected in subsequent stages to fragmentation, consolidation and plastic working. The ribbons and extruded rods cast were described in terms of their structure and their strength properties were determined at different measurement temperatures. It was shown that the lightweight materials produced from aluminium alloys using the rapid solidification process have an ultra-fine structure and good strength properties.

Analysis under a microscope confirmed that the addition of rare earth alloys Al-Si and Al-Si-Ni causes fragmentation of the microstructure in the tapes produced. The presence of rare earth elements in the alloys tested has an impact on the type and the morphology of the particles of the microstructure's individual components. In addition to the change in particle morphology, the phenomenon of the separation of numerous nanometric particles of intermetallic phases containing rare earth elements was also observed. The change in microstructure caused by the addition of rare earth elements in the form of a mischmetal increases the mechanical properties.

Keywords: aluminium alloy, rapid solidification, grain refinement, ultrafine structure

1. Introduction

Aluminium alloys are a very attractive construction material due to their properties, in particular high relative strength. For this reason, they are widely used in many industries. However, the increasing competition and requirements for construction materials contribute to the search for new, higher mechanical properties of aluminium alloys and their production techniques.

It is well known that the mechanical properties of alloys depend to a large extent on the chemical composition as well as the method and parameters of their production. These properties depend on the structure, which can be altered, for example, by changing the chemical composition, the cooling rate during casting, and by plastic working or heat treatment. The Hall-Petch relation indicates that the decrease of grain size causes an increase in strength properties, which is often achieved without the loss of plastic properties. In addition, the introduction of some alloy additives allows to increase the stability of the structure and improve the properties at elevated temperatures. Such elements may include silicon, nickel, zirconium, chromium or rare earth elements [1-7].

Research [8-11] show that Al-Si alloys with the addition of Ni and rare earth elements, and in particular Ce, having an ultrafine, nanocrystalline or amorphous structure, are characterised by high strength, hardness and resistance to abrasion at elevated temperatures.

Among all the aluminium alloy production methods, rapid solidification that allows obtaining materials with a finely divided structure seems very promising. We can distinguish several methods, but melt-spinning deserves special attention. This method allows for the production of materials with an ultrafine structure, which are nanocrystalline, nanoquasicrystalline and sometimes amorphous [8]. Thus, these materials are attractive due to the high mechanical properties achieved. In addition, this method allows for the production of materials with compositions that are difficult or impossible to achieve using traditional metallurgy. Melt-spinning involves rapid cooling of liquid metal by

[1] ŁUKASIEWICZ RESEARCH NETWORK – INSTITUTE OF NON FERROUS METALS, 19 PILSUDSKIEGO STR., 32-050 SKAWINA, POLAND
[2] AGH UNIVERSITY OF SCIENCE AND TECHNOLOGY, ACADEMIC CENTRE FOR MATERIALS AND NANOTECHNOLOGY, AL. MICKIEWICZA 30, 30-059 KRAKÓW, POLAND
[3] AGH UNIVERSITY OF SCIENCE AND TECHNOLOGY, FACULTY OF FOUNDRY ENGINEERING, 23 REYMONTA STR., 30-059 KRAKÓW, POLAND

* Corresponding author: dkapinos@imn.skawina.pl

feeding it into a spinning wheel in the form of a thin stream. The spinning wheel made of copper cooled with water dissipates heat as a result of which alloy solidifies and a ribbon or thin flakes form. In order to obtain massive materials from small-sized ribbons (thickness 50-200 μm and width 2-30 mm) it is necessary to apply consolidation processes, i.e. pressing and hot extrusion or forging [9-17].

The aim of this paper is to determine the effect of the addition of rare earth elements on the microstructure and mechanical properties of near-eutectic Al-Si-Ni alloys after rapid crystallization and consolidation.

2. Methodology

Using an unconventional rapid solidification method, ultrafine Al-Si and Al-Si-Ni alloys with the addition of rare earth elements (Ce, La, Nd, Pr) were produced and the impact of the chemical composition and parameters of the alloys production on their structure and properties was determined.

The tests were carried out using four aluminium alloys containing silicon in the amount of approx. 12.6 wt% (near-eutectic silumins) with the addition of nickel in the amount of approx. 13 wt% and rare earth elements in the form of a mischmetal (Mm) in the amount of approx. 4-5 wt%. The applied mischmetal contained a mixture of Ce (approx. 50 wt%), La (approx. 26 wt%), Nd (approx. 22 wt%) and Pr (approx. 2 wt%).

The alloys were prepared in an induction furnace. Mischmetal, silicon and nickel in pure form was successively added to the molten aluminium with a purity of 99.8% at the appropriate temperature (Tab. 2). The prepared alloys were cast into a steel metal mould. The chemical composition of alloys is shown in Tab. 1.

TABLE 1

Chemical composition of produced ribbons

Element	Content, wt%			
	AlSi12	AlSi12 Mm4	AlSi12 Ni13	AlSi12 Mm5Ni13
Si	12.46	12.65	12.74	12.53
Ni	0.00	0.01	12.97	12.51
Pr	0.00	0.17	0.00	0.19
Ce	0.00	2.00	0.00	2.62
La	0.00	1.24	0.00	1.42
Nd	0.00	0.57	0.00	0.62
Fe	0.12	0.18	0.24	0.13
Mn	0.03	0.09	0.07	0.00
Mg	0.00	0.00	0.01	0.00
Cu	0.00	0.00	0.00	0.00
Zn	0.02	0.02	0.02	0.01
RE (total)	0.00	3.98	0.00	4.85

A thermal analysis was carried out on the alloys produced with the appropriate chemical composition to determine the appropriate casting temperature (Tab. 2).

TABLE 2

Casting parameters of the alloys tested

Casting parameters	AlSi12	AlSi12 Mm4	AlSi12 Ni13	AlSi12 Mm5Ni13
Temperature at the end of solidification, °C	567	557	548	548
Temperature at the beginning of solidification , °C	578	622	645	790
Melt pouring temperature, °C	640	680	700	850
Temperature of the nozzle – valve, °C	640	680	700	860

A thermal analysis was carried out on the alloys produced with the appropriate chemical composition to determine the appropriate casting temperature (Tab. 2).

For all alloys tested, the difference between casting temperature and liquidus temperature was about 60°C. Pre-prepared alloys were melted in an induction furnace and then poured into a crucible located in the melt spinner. The casting parameters of the alloys were determined based on previous tests [1,4,10,12] and data from source literature. The alloys tested were cast at:

– Constant linear speed of ribbon casting of 30 m/s,
– Uniform diameter of the nozzle of 1,2 mm,
– Pressure of the gas ejector pushing the metal of 20-40 kPa,
– Constant temperature of the crystallizer wheel of 20°C,
– Application of a filter with density of 20 ppi.

The microstructure of a cross-section of ribbons produced was analysed using a transmission electron microscope (TEM) TECNAI G20. Thin films were prepared directly from the ribbons, which were polished on both sides and then electropolished in 330 mlHNO_3 + 660 mlCH_3OH reagent. A series of photographs was taken and the size of grain in all samples and s-DAS (Secondary Dendrite Arms Spacing) for samples containing 13% Ni was measured using the secant method.

The ribbons cast, which are an intermediate product, were later subjected to fragmentation and plastic working. The fragmentation process was carried out using the TRIA XT 50-30 mill with a screening sieve with a mesh diameter of ø3 mm.

The plastic working process consisted of the initial cold consolidation of the crushed ribbons with the force of 350-400 kN. This force was sufficient to obtain well consolidated mouldings with a diameter of 40 mm. The mouldings prepared in this manner were heated to 450°C (for Al-Si and Al-Si-Mm alloys) and 525°C (for Al-Si-Ni and Al-Si-Ni-Mm alloys) and rods with a diameter of ø8 mm were extruded in the concurrent hot extrusion process at 1 mm/s and force of v = 40-55 T. Both processes were carried out using a vertical press with a maximum force of 1000 kN.

The resulting rods with a length of 40-50 cm had a smooth surface without tears and cracks. After assessing their fractures, it can be concluded that the hot consolidation parameters were selected correctly.

Microsections were prepared from the cross-section of extruded rods with a diameter of ø8 mm, which were subjected

to the analysis of crystallographic orientation (Electron Back-Scatter Diffraction – EBSD) using an EBSD camera. All scans were made in size 7×7μm with a step of 150 nm.

Thin films were prepared from the cross-section of the rods, which were then dimpled to obtain perforations, and then ion etched on the RES101 ionic extractor. Tests were carried out using a transmission electron microscope (TEM) Tecnai G2 with an EDS adapter and HAADF detector. The microstructure of the samples was analysed using a transmission microscope, the grain and sub-grain size was measured using the secant method and phases in micro-areas were subjected to chemical analysis. Diffraction analysis was carried out with Sleeve 4+ software using the PDF4+ database from 2016.

3. Results and discussion

Thin ribbons were produced using melt spinning. The cooling rate in the melt spinner is of the order of 10^4-10^6°C/s. The average alloy ribbon thickness was similar and ranged from 57 to 68 μm. The thickness distribution of the ribbons was also similar and ranged from 40-90 μm. The width of the ribbons was 1.5-3 mm.

During the casting, variable cooling parameters of the ribbons occur, heat during the alloy crystallization is discharged faster on the side of the wheel compared to the atmosphere side, i.e. the air. Therefore, the ribbons differed in the surface topography, and the microstructure on the crystallizer surface side was more fragmented in relation to the microstructure on the atmosphere side.

A compression test was carried out on extruded ø8 mm rods at ambient temperature and at 200, 300 and 400°C. The test was carried out on samples ø5 × 7.5 mm with a deformation equal to 60%.

3.1. Evaluation of the microstructure of ribbons produced using rapid solidification (RS)

The microstructure of samples taken directly from the ribbons post-RS was analysed using the TEM with EDS and HAADF detectors.

The analysis of the AlSi12 sample's microstructure shows that small grains of approximately 2 μm are formed after RS (Fig. 1a, Tab. 3). The grain boundaries have a high saturation of Si precipitates, which form a dark "network" on grain boundaries/dendrites. Grains have round shapes, most often they are round or elliptical, elongated in one direction. In Fig. 1b, grain is visible, inside which a large number of Si precipitates of nanometric size can be observed.

The microstructure of AlSi12Mm4 samples in relation to the microstructure of the AlSi12 sample was characterised by a similar shape and grain size (Fig. 2). Inside the grains and at the boundaries, apart from the minor rhombic Si solid solution, there were also rod-shaped precipitates, which formed after adding mischmetal in the amount of 4 wt% to the alloy. These precipitates, however, were not observed in the AlSi12 sample.

After casting, the AlSi12Ni13 sample had a typical dendritic microstructure but its size was far from typical cast structures. The average s-DAS size was about 100 nm while the dendrite grain was about 1 μm. In addition, by performing diffraction from the area (Fig. 3a and b), it was observed that diffraction rings appear against the background of the crystal lattice spots, which probably comes from amorphous structures. Diffraction spots suggest crystalline structure which is inside dendritic grains, so the amorphous structure probably occurs in the areas between dendrites.

Chemical analysis has shown that there is very high saturation of Si and Ni in the areas between the dendrite arms (Fig. 3b). This eutectic area probably shows a partial amorphisation of the structure.

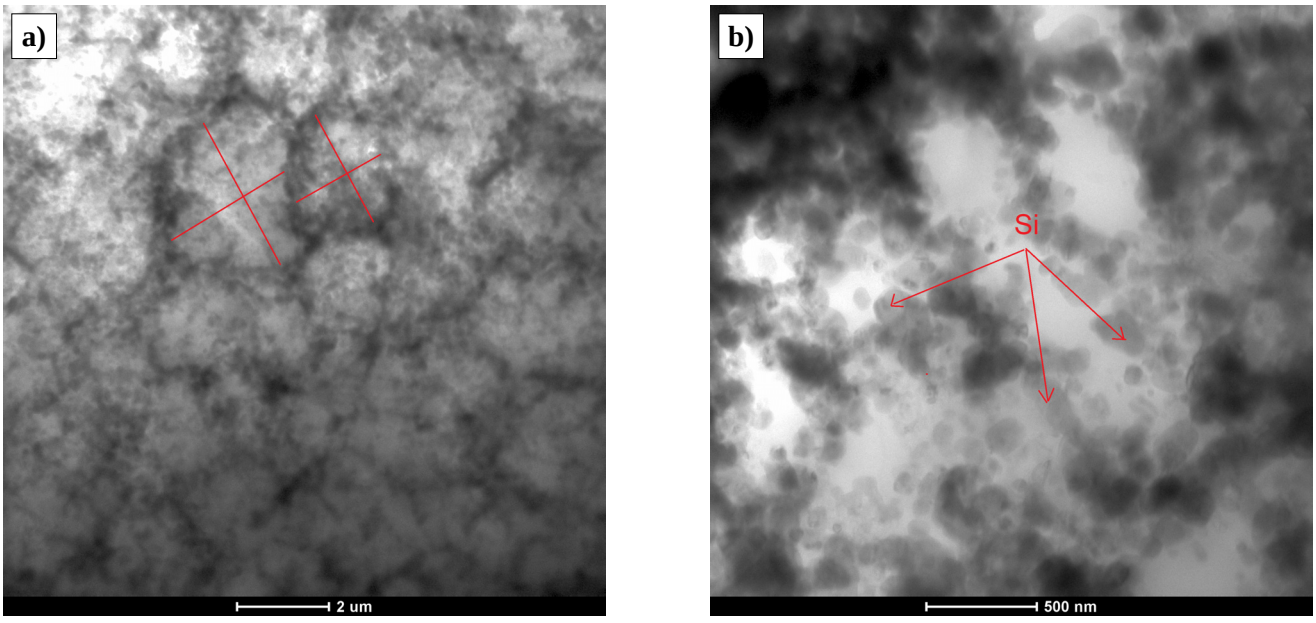

Fig. 1. Bright-field TEM images of the AlSi12 alloy, a) selected grain size, b) selected Si precipitates

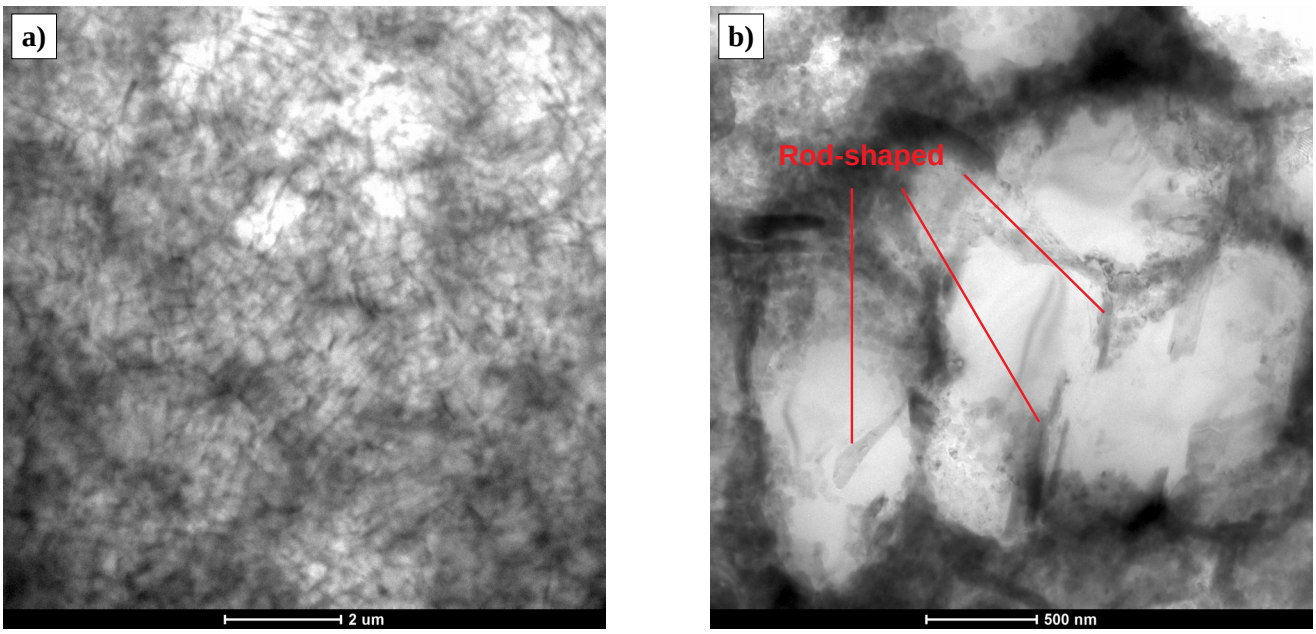

Fig. 2. Bright-field TEM images of the AlSi12Mm4 alloy

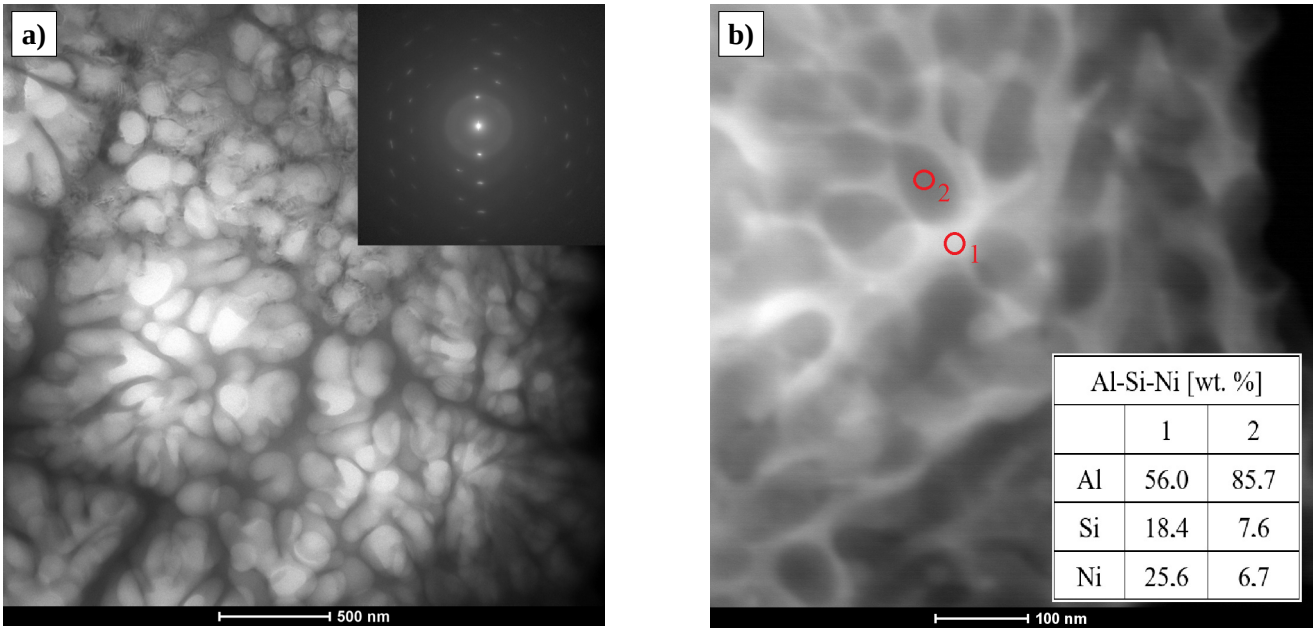

Fig. 3. a) Bright-field TEM images with corresponding SADPs of the AlSi12Ni13 alloy and b) STEM image with point chemical analysis

Analysis of the AlSi12Ni13Mm5 alloy sample reveals its nanometric microstructure (Fig. 4). The appearance of the microstructure has not changed in terms of its shape as a result of adding 5 wt% of Mm (Fig. 4). A dendritic structure was still visible, however, even finer than in the sample without Mm. The size of the dendrite grain reached approx. 800 nm and the s-DAS measurement showed 50 nm. Similarly to the AlSi12Ni13 alloy sample, the structure was partly amorphous because the spots from the crystallographic lattice together with the circles probably from the amorphous structure overlapped (Fig. 4). Differences in diffraction between samples with and without Mm were also found in the distribution of spots. Spots on the diffraction of the AlSi12Ni13Mm5 alloy sample were partially distributed over the circles, indicating the diffraction of more grains. Very small precipitations below 20 nm were very rare

TABLE 3

Average grain size and s-DAS

		AlSi12	AlSi12 Mm4	AlSi12 Ni13	AlSi12 Ni13Mm5
*Grain	Average, nm	2350	2225	1021	798
	Deviation	900	537	386	277
**s-DAS	Average	464	278	98	49
	Deviation	11	12	15	11

* Grain – area surrounded by a high angle grain boundaries > 15 degrees
** s-DAS – Secondary Dendrite Arms Spacing

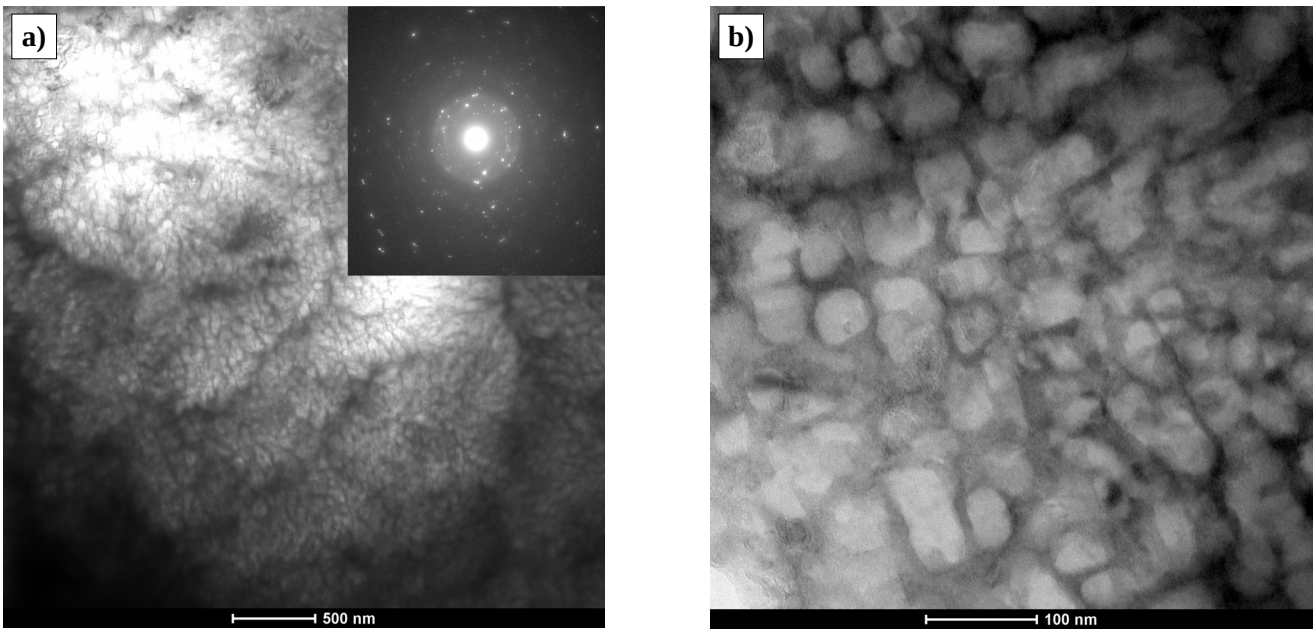

Fig. 4. Bright-field TEM images with corresponding SADPs of the AlSi12Ni13Mm5 alloy

in the structure. The point chemical analysis shows that the interdendritic areas contain a high saturation with elements such as Si, Ni, La, Ce and Nd, while dendrite interiors are mainly composed of the α – Al solution.

Measurement of the average grain size using the TEM microscope showed that AlSiNi and AlSiNiMm alloys containing 13 wt% of nickel have the most finely fragmented structure. The addition of mischmetal in the amount of 4-5 wt% to the AlSi and AlSiNi alloys resulted in a grain size reduction by approx. 5 and 20%.

3.2. Evaluation of microstructure of the rods produced after the plastic working process

Fig. 5 shows the results of the EBSD metallographic orientation analysis. Scans were made only for the aluminium matrix, omitting the remaining phases.

The analysis of the EBSD orientation distribution maps for rods after the extrusion process showed that the largest grain size occurs in the AlSi12 alloy (≤2 μm) (Fig. 5). The addition of mischmetal to this alloy caused a reduction in grain size (AlSi12Mm4 alloy). However, the grain size in nickel alloys is the smallest (≤1 μm). It can also be seen that for the first two alloys, without the addition of nickel, the crystallographic orientation is similar and mainly includes the direction families (111) and (001) as opposed to alloys with the addition of nickel. This may be related to the dynamic recrystallization that took place during the extrusion process at a temperature higher by 75°C for alloys with the addition of Ni.

The microstructure of post-RS rod samples was analysed using the TEM with EDS and HAADF detectors.

The microstructure of the AlSi12 sample had fine sub-grains of approx. 800 nm (Fig. 6a). Si precipitates were visible at the sub-grain boundaries, with the size between 200 and 600 nm. Si precipitates had rhombohedral shape, twins and stacking faults were visible inside them.

The addition of 4 wt% of Mm to the AlSi12 alloy changed the microstructure's appearance and did not influence the greater sub-grain fragmentation because the average sub-grain

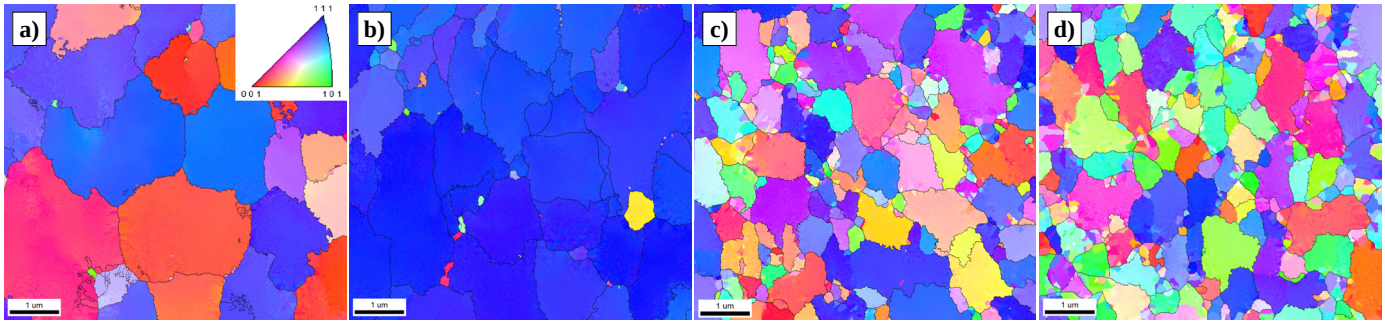

Fig. 5. Coloured inverse pole figure (IPF) maps obtained from EBSD analysis showing the grain size in investigated alloys where the colour corresponds to the crystallographic orientation shown in the standard stereographic triangle (inset)

size was about 750 nm (Fig. 7a). The distribution and size of precipitates within the sub-grains has changed. New precipitates appeared, generating a higher density of dislocations. Fig. 7b and 7c shows the electron diffraction and spot chemical composition confirming the occurrence of $Le_{0.5}Ce_{0.5}Si$ precipitates with crystal structure a = 0.836 nm, b = 0.399 nm, c = 0.601 nm; $\alpha, \beta, \gamma = 90°$; space group – Pnma (62). The size of these precipitates did not exceed 500 nm and their shape resembled prisms with rounded edges. In addition, Si precipitates similar in shape and size were observed just like in the alloy without the addition of Mm.

The AlSi12 alloy's microstructure with the addition of 13 wt% of Ni is significantly different from the AlSi12 and AlSi12 alloy samples with the addition of 4 wt% of Mm (Fig. 8). The average grain size measured using the secant method was approx. 760 nm and did not change compared to the sample containing the addition of 4 wt% of Mm. The precipitates formed as a result of the eutectic transformation during the fast crystallization process show spherical shapes and their largest size (diameter) is similar to the average size of the sub-grains in the alloy. The analysis of electron diffraction and the chemical composition using the TEM shows that these are the Al_3Ni phases with crystal structure a = 0.660 nm, b = 0.735 nm, c = 0.480 nm; $\alpha, \beta, \gamma = 90°$; space group – Pnma (62) (Fig. 8b and c). As in the previous samples, the Si phase was present in shapes and sizes similar to those described in the AlSi12 alloy sample. No twins or stacking faults were found in the Si precipitates.

The AlSi12 alloy's microstructure with 13 wt% of Ni and 5 wt% of Mm was characterised by sub-grains similar to other alloys and a large number of precipitates of various shapes and sizes (Fig. 9). Based on chemical analyses in fine longitudinal precipitates, a varying occurrence of the elements La, Ce and Nd with a high content of Ni and Si was observed. The analyses of high-resolution images and electron diffraction revealed that, in addition to the Si and Al_3Ni phases, Al_4CeNi (with crystal structure a = 0.414 nm, b = 1.585 nm, c = 0.664 nm; $\alpha, \beta, \gamma = 90°$; space group – Cmcm (63)) as well as $La_{0.33}Ce_{0.40}Nd_{0.27}Ni_{4.2}Al_{0.8}$ (with crystal structure a = 0.501 nm, b = 0.501 nm, c = 0.406 nm; $\alpha, \beta = 90°$, $\gamma = 120°$; space group – P6/mmm (191)) phases occur in the alloy. However, these phases did not contain Si, which could occupy positions in interstitial spaces or exchange positions with Al or Ni. Phases containing Si and Ni as well as rare earth elements were not shown in the latest crystallographic database PDF4+ 2016.

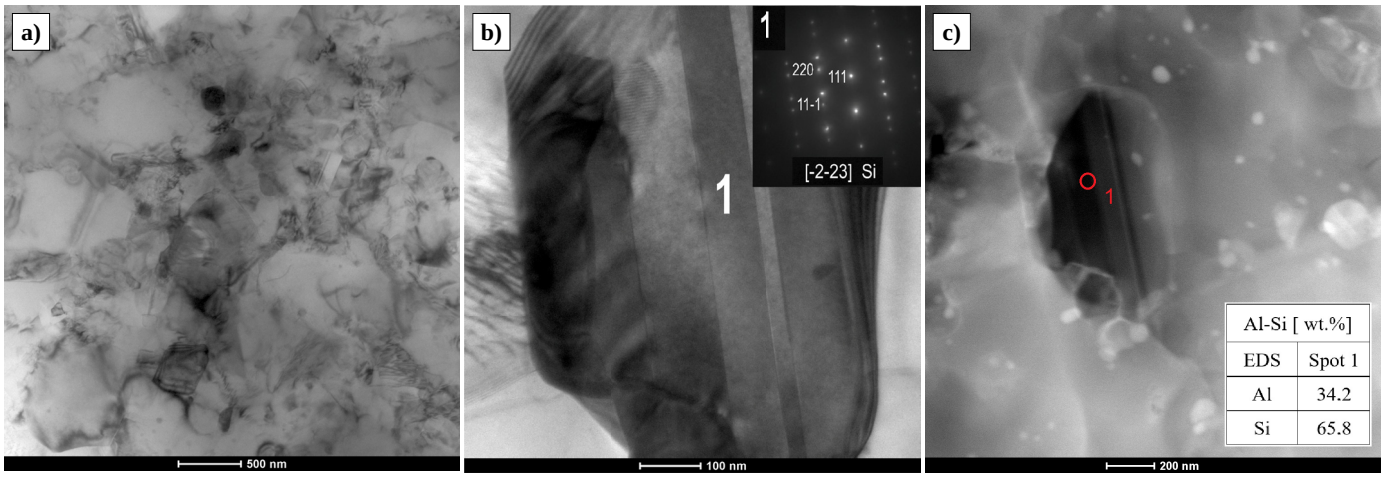

Fig. 6. a), b) Bright-field TEM images with corresponding SADPs of the AlSi12 alloy and c) STEM image with point chemical analysis

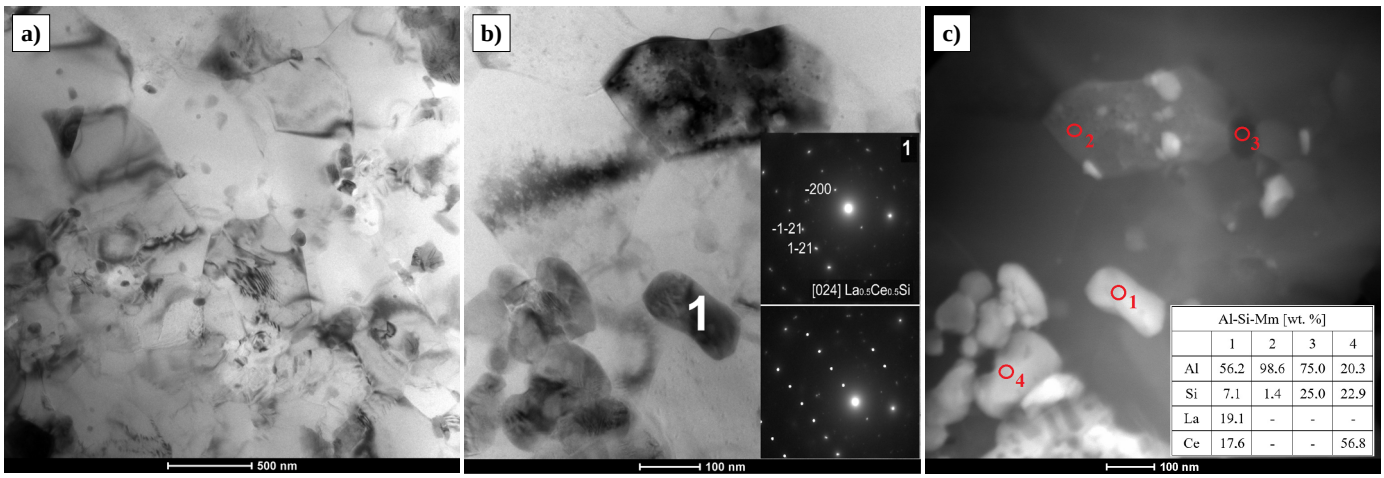

Fig. 7. a), b) Bright-field TEM images corresponding SADPs pattern and simulation of $Le_{0.5}Ce_{0.5}Si$ phases and c) STEM image with point chemical analysis of the AlSi12Mm4 alloy

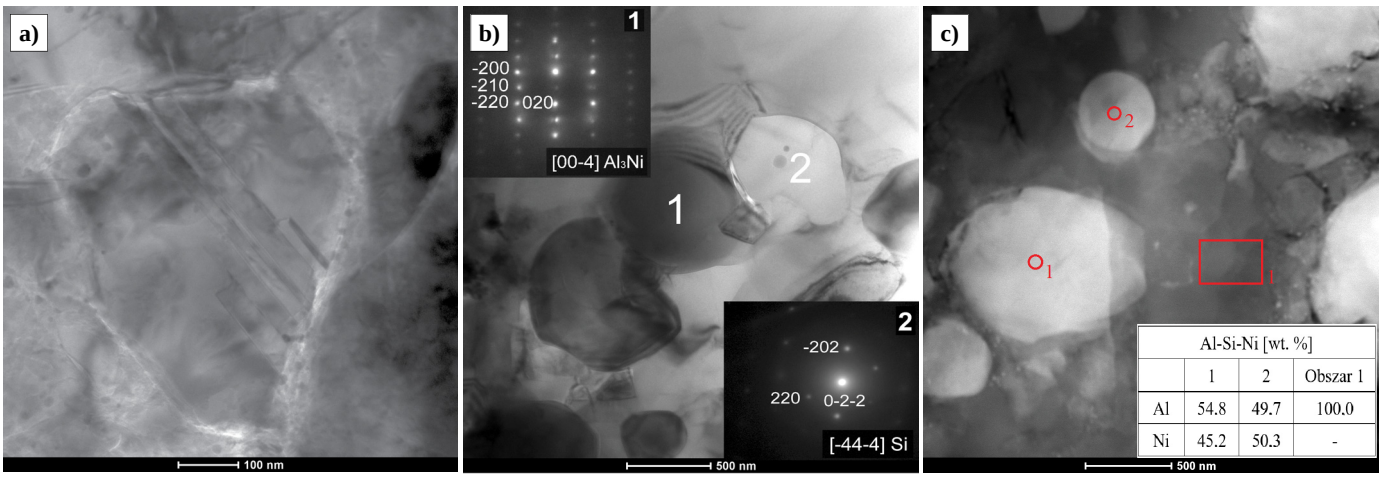

Fig. 8. a), b) Bright-field TEM images corresponding SADPs pattern and simulation of Al_3Ni and Si phases and c) STEM image with point chemical analysis of the AlSi12Ni13 alloy

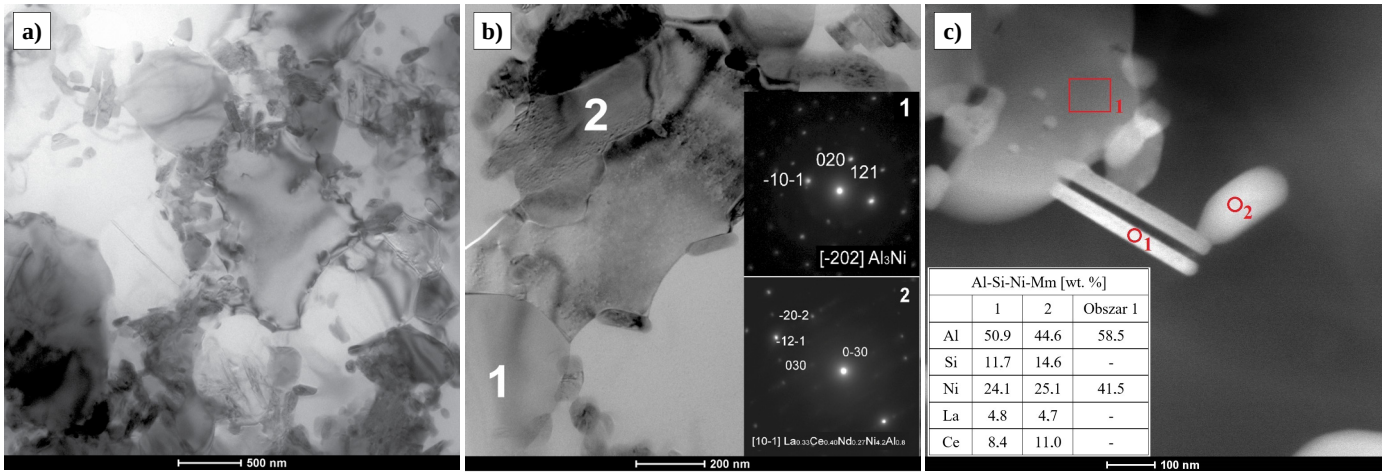

Fig. 9. a), b) Bright-field TEM images corresponding SADPs pattern and simulation of of Al_3Ni and $La_{0.33}Ce_{0.40}Nd_{0.27}Ni_{4.2}Al_{0.8}$ phases and c) STEM image with point chemical analysis of the AlSi12Ni13Mm5 alloy

Tab. 4 shows the cumulative results of the average sub-grain size for the samples tested.

There were no large differences in the sub-grain size đ ~ 770 nm between samples of the tested alloys.

TABLE 4

Results for the average size of the sub-grain

	AlSi12	AlSi12 Mm4	AlSi12 Ni13	AlSi12 Ni13Mm5
*Sub-grain, nm	812.4	755.9	765.6	742.2
Deviation	436.5	475.1	319.9	416.3

* Sub-grain – area surrounded by a low and high angle grain boundaries

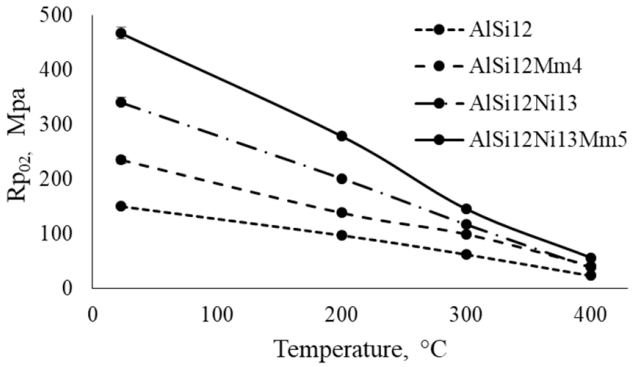

Fig. 10. The yield point of the tested alloys depending on the temperature

3.3. Evaluation of strength properties in a compression test at elevated temperatures

Fig. 10 sums up the results for strength properties from the compression test at elevated temperatures.

On the basis of the obtained results, it can be stated that for all tested alloys, the temperature increase causes an even decrease in strength properties. The addition of both nickel and rare earth elements in the form of mischmetal to the Al-Si alloy caused a significant increase in yield strength and stress at 60% deformation. The addition of rare earth elements in the form

of mischmetal to the Al-Si alloy caused an increase in $R_{p0.2}$ by approx. 50% and $R_{m60\%}$ by approx. 25%, while for the Al-Si-Ni alloy it increased the yield point by nearly 40% and stress by approx. 5%. The best strength properties in the compression test carried out at temperatures were obtained for the AlSi12Ni13Mm5 alloy.

4. Conclusions

Ribbons cast from the tested alloys had a diversified ultrafine dendritic microstructure. Alloys AlSi12Ni13 and AlSi12Ni13Mm5 containing rare earth elements and nickel had a smaller average grain size of đ ~ 1000-800 nm, compared to the alloy AlSi and AlSiMm, where the value was ð ~ 2350-2200 nm.

EBSD maps showed, identically to the ribbons, that rods containing alloys containing rare earth elements and nickel have a more fragmented structure compared to AlSi alloys. However, the average size of the sub-grains measured on the electron microscope in the rods produced from the tested alloys was similar and amounted to ð ~ 770 nm.

The Si and Al_3Ni phases were observed in the AlSi12 and AlSi12Ni13 alloys, in alloys containing Mm additions, the following phases were released: $La_{0.5}Ce_{0.5}Si$, Al_4CeNi and $La_{0.33}Ce_{0.40}Nd_{0.27}Ni_{4.2}Al_{0.8}$. Precipitates containing rare earth elements were characterised by a fine structure and were mostly observed at the grain boundaries.

The strength tests carried out in form of compression tests at elevated temperatures show that the rods produced have good strength properties. The addition of both nickel and rare earth elements in the form of mischmetal to the Al-Si alloy caused an increase in the yield point $R_{p0.2}$ by about 25-50% and strain $R_{m60\%}$ by about 5-25%.

These results suggest that the high strength of Al-Si alloy rods was obtained by adding TM transition elements, such as Ni and RE, by the precipitation of nanometric reinforcing intermetallic phases evenly distributed in the matrix consisting of aluminium and silicon grains.

REFERENCES

[1] M. Szymanek, B. Augustyn, D. Kapinos, J. Żelechowski, M. Bigaj, Al-Si-RE alloy cast in the Rapid Solidification, Archives of Metallurgy and Materials **60**, 4, 3045-3050 (2015). DOI:10.1515/amm-2015-0488

[2] A. Kukuła-Kurzyniec, J. Dutkiewicz, P. Ochin, L. Perriere, P. Dluzewski, A. Góral, Amorphous - Nanocrystalline Melt Spun Al-Si-Ni Based Alloys Modified with Cu and Zr, Archives of Metallurgy and Materials **58**, 2, 419-423 (2013). DOI: 10.2478/amm-2013-0010.

[3] A. Inoue, K. Othera, A.P. Tsai, T. Masumoto, J. Jpn. Appl. Phys. **27**, L280 (1998).

[4] B. Augustyn, M. Szymanek, D. Kapinos, W. Pakieła, Evaluation of Functional Properties of the Rapidly Solidified Cast AlSi30 Alloy as a Material for Transport Applications, Light Metals 2014, 975-980, ISSN 1096-9586 (2014).

[5] F.H. Froes, S.J. Savag, Processing of structural metals by rapid solidification ASM International, 475 ISBN 0871702924 (1987).

[6] T.K. Croat, A.K. Gangopadhyay, K.F. Kelton, Crystallization in Al88RE8Ni4 Glass Forming Alloys, Department of Physics, Washington University, One Brookings Drive, Campus Box 1105, St. Louis, Mo 63130-4899 (2001).

[7] K.L. Sahoo, A. Mitra, S. Ghosh, Efect of rare-earth elements on nanophase evolution, crystallization behaviour and mechanical properties in Al-Ni-R (R = La/Mischmetal) amorphous alloys, Pramana journal of physics. Indian Academy of Sciences **65**, 4, 745-751 (2005).

[8] T.H. Lee, S.J. Hong, Microstructure and mechanical properties of Al-Si-X alloys fabricated by gas atomization and extrusion process, Journal of Alloys and Compounds **487**, 218-224 (2009)

[9] T.H. Lee, Y. Kawamura, A. Inoue, S.S. Cho, T. Masumoto, Mechanical properties of rapidly solidified Al-Si-Ni-Ce P/M alloys, Scripta Materialia **36**, 475-480 (1997).

[10] I. Johansen, H.J. Roven, Mechanical properties of a rapidly solidified Al-Si-Ni-Mn alloy, Materials Science and Engineering A **179-180**, 605-608 (1994).

[11] E.R. Wang, X.D. Hu, S.S. Wang, Y.F. Zhao, G.L. Chen, Microstructure and mechanical properties of Al–Si–Ni–Ce alloys prepared by gas-atomization spark plasma sintering and hot-extrusion, Materials Science and Engineering A **528**, 5764-5771(2011).

[12] A. Inoue, Amorphous, nanoquasicrystalline and nanocrystalline alloys in Al-based systems, Progress in Materials Science **43**, 365±520 (1999).

[13] J. Latuch, T. Kulik, Two-phase nanocrystalline-amorphous aluminum alloys (in Polish), Inżynieria materiałowa **4**, 194-198 (2005).

[14] M. Szymanek, B. Augustyn, D. Kapinos, S. Boczkal, J. Nowak, Producing Ultrafine Grain Structure in AZ91 Magnesium Alloy Cast by Rapid Solidification. Archives of Metallurgy and Materials **59**, 1, 317-321 (2014). DOI:10.2478/amm-2014-0052.

[15] C. Suryanarayana, A. Inoue, Bulk Metallic Glasses, CRC Press. Boca Baton, 382 (2012).

[16] M. Szymanek, B. Augustyn, D. Kapinos, S. Boczkal, J. Nowak, The Production of Material with Ultrafine Grain Structure in Al-Zn Alloy in the Process of Rapid Solidification, Archives of Foundry Engineering **14**, 2, 57-62 (2014). ISSN 1897-331.

[17] S.J. Hong, B.S. Chun, Material Science Enginiering A**348**, 262-270 (2003).

[18] H.S. Kim, Y.H. Sohn, T.G. Kim, J.M. Koo, S.J. Hong, Thermal Stability, Microstructure and Mechanical Properties of Nanostructured Al-Ni-Mm-X (X = Cu and Fe) Alloys Hot-Extruded from Gas-Atomized Powders. Materials Transactions **49**, 6, 1223-1228 (2008).

[19] Y. Kawamura, H. Mano, A. Inoue, Scripta Matererialia **44**, 1599 (2001).

[20] I. Börner, J. Eckert, Scripta Matererialia **45**, 237 (2001)

[21] P. Todeschini, G. Champier, F.H. Samuel, Production of Al-(12-25) wt % Si alloys by rapid solidification melt spinning versus centrifugal atomization, Jurnal of Material Science **27**, 3539-3551 (1992).